

# Effects of processing parameters on microstructures of TiO<sub>2</sub> coatings formed on titanium by plasma electrolytic oxidation

Chunwen Sun · Rob Hui · Wei Qu ·  
Sing Yick · Colin Sun · Weimin Qian

Received: 9 April 2010/Accepted: 14 June 2010/Published online: 26 June 2010  
© Springer Science+Business Media, LLC 2010

**Abstract** Titanium oxide (TiO<sub>2</sub>) coatings were formed on titanium substrates in a sodium silicate (Na<sub>2</sub>SiO<sub>3</sub>) aqueous solution, using plasma electrolytic oxidation method. The effects of duty ratio, frequency, and positive/negative pulse proportion on the microstructure and phase compositions of the coatings were investigated. The coatings were mainly composed of anatase TiO<sub>2</sub> plus a little amount of rutile TiO<sub>2</sub>. The coatings obtained at the frequency range 900–2700 Hz, under a duty ratio of 20%, and a positive/negative pulse proportion of 3, showed the best quality in terms of density and adhesion. The effect of positive/negative pulse proportion was relatively small. However, continuous coating could not be obtained using the positive/negative pulse proportion of 1. Compared with that of bare titanium, the property of resistance to corrosion was obviously improved for the titanium with TiO<sub>2</sub> coating. The corrosion potential rose about 0.13 V and the corrosion current density decreased about one order of magnitude.

## Introduction

Titanium and its alloys are widely used in the aerospace [1, 2], automobile [3], biomedical [4–6], energy industry [7], and military applications [8] due to their high strength, high-melting point, and good biocompatibility. However, poor corrosion and tribological properties are the

disadvantages of these materials, and therefore they are usually used with protective coatings [9, 10]. In recent years, several different coating approaches have been utilized for the fabrication of coatings on titanium or its alloys, such as plasma spraying [11], microwave-assisted self-propagating high-temperature technique [12], electrochemical anodization treatment [13], sol–gel method [14–16], electron beam physical vapor deposition [17], and so on. However, most of these methods need expensive apparatus, or time-consuming, or high-temperature treatment that limits their applications to thermally stable coatings. Plasma electrolytic oxidation (PEO), also called micro-arc oxidation, pulse plasma anodization, or spark anodization, is an emerging environmentally benign technology to produce wear- and corrosion-resistant ceramic coatings on aluminum (Al), magnesium (Mg), titanium (Ti), zirconium (Zr), and other light metals as well as their alloys [18–20]. PEO method uses the effects of forming micro-arc plasma discharges on the surface of the workpieces treated in aqueous electrolytic solution. Because of influences of the discharges on the workpieces, a multi-function protective ceramic coating forms with unique properties including very high hardness, excellent wear resistance, excellent corrosion resistance, extremely high adhesion property, dielectric property, and high thermal shock resistance. In PEO treatment, two modes are usually used, i.e., a direct-current (DC) mode and an alternating-current (AC) mode. It is believed that the AC mode is more effective to form the coatings than DC mode [21–26]. An asymmetric AC power has been used to deposit ceramic coatings on pure Ti and Ti–6Al–4V alloy by Yerokhin et al. [18, 22] and Xue et al. [23]. Yerokhin et al. [22] found that the AC mode provides more intensive sparking on the surface and partial reduction and dissolving of some oxide compounds during the negative half-cycles. This

C. Sun (✉) · R. Hui · W. Qu · S. Yick · C. Sun · W. Qian  
Institute for Fuel Cell Innovation, National Research Council  
Canada, 4250 Wesbrook Mall, Vancouver, BC V6T 1W5,  
Canada  
e-mail: Springwensun@yahoo.com.cn;  
chunwen.sun@nrc-cnrc.gc.ca

promoted formation on the surface of the rutile phase, lower valent oxides, and intermetallics as well as hindering penetration of electrolyte anions in the film.

It has been found that the electrical parameters and electrolyte composition play key roles in the PEO process. Han et al. [27] investigated preparing titania-based coatings on titanium substrate by PEO in electrolytic solutions containing four different electrolyte solutions. They found that the morphology and phase components of the coatings strongly depending on the electrolytes composition and the applied voltage. Wang et al. [9] found that rutile phase in the coating increases and becomes the predominant phase with the duty ratio increases from 4 to 20%. Yao et al. [28] investigated the effects of duty ratio at low frequency. They found the changes of duty ratio led to the changes of the mode of the spark discharge and further influenced the structure and morphology of the ceramic coatings for the pulsed single-polar micro-plasma oxidation. By controlling various process parameters, the microstructure and composition of coatings can be optimized. The corrosion and wear resistance properties of titanium and its alloys can thus be improved. Until now, there have been few reports on the systematical investigation of the effects of various process parameters on the microstructure and corrosion-resistant properties of titanium oxide ( $TiO_2$ ) coatings. In this article, the effects of duty ratio, frequency, and positive/negative pulse proportion on the PEO coatings formed on titanium substrate are investigated. The corrosion behavior was also evaluated by potentiodynamic polarization measurements.

## Experimental

Commercially pure titanium plate (Grade 2, R50400) was cut into samples with dimensions of  $50\text{ mm} \times 10\text{ mm} \times 1\text{ mm}$ . The compositions of impurity in Ti plate are C 0.08 wt%, O 0.18 wt%, N 0.03 wt%, H 0.015 wt%, and Fe 0.30 wt%. Prior to the PEO treatment, the specimens were polished with 400 grit SiC abrasive paper, and degreased with acetone and then rinsed with deionized water. A home-made pulsed power source was used for the PEO treatment of the samples. The PEO unit mainly consists of a water-cooled glass electrolyser with stainless steel liner and a high power electrical source. The stainless steel liner also serves as the counter electrode. The electrolyte solution in this study is an aqueous solution consisted of  $27\text{ g L}^{-1}$  sodium silicate ( $Na_2SiO_3$ ). After the treatment, the coated samples were rinsed with deionized water and dried in air.

The pulse output of the power supply unit for the PEO treatment is schematically shown in Fig. 1. The pulse duty ratio is defined as follows:

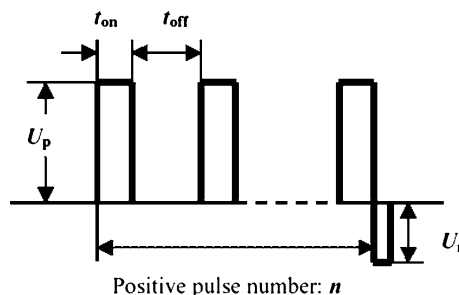


**Fig. 1** An illustration of the pulse output of the PEO

$$\text{Duty ratio } (D) = \frac{t_{on}}{t_{on} + t_{off}} \times 100\%$$

where  $t_{on}$  is the pulse on-time and  $t_{off}$  is the pulse off-time. In this study, the negative pulse duty ratio  $D_n$  was set as 10%; negative pulse voltage  $U_n$  was fixed as 12 V; the number of negative pulse was 1, namely, a cycle of  $n$  positive pulse was followed by one negative pulse. For simplicity, the duty ratio and positive/negative pulse proportion are hereafter abbreviated as  $D$  and  $R$ , respectively. To study systematically the effects of the frequency, duty ratio, and positive/negative pulse proportion on the coating microstructure, phase composition, and growth kinetics of the coatings, a constant current mode was used at an average current density of  $0.12\text{ A cm}^{-2}$  in all depositions. The total time for PEO treatment was 2.5 h.

The phase composition of coatings was examined by X-ray powder diffraction performed on Bruker AXS D8 Advance with  $Cu K\alpha$  radiation. The morphology of the surfaces and cross sections of the coatings was characterized by a scanning electron microscope (SEM, Hitachi S-3500 N, Japan) with an accelerating voltage 20 kV. For the preparation of the cross section, the sample was cut, mounted, and solidified by the epoxy, then polished. Prior to the SEM examinations, the samples were coated with gold by sputtering to minimize the charging effects under SEM imaging conditions. Chemical compositions and elemental distributions were analyzed by X-ray energy dispersion spectroscopy (EDS) coupled to the SEM (Oxford, UK). The coating thickness was measured by a thickness gauge (CTG-10, Company, USA) with a minimum resolution of 1  $\mu\text{m}$ . The average thickness of each sample was obtained from five measurements at different positions. Real-time imaging of the micro-discharges was monitored using a digital video to show its spatial distribution, size, density, and lifetime during the PEO treatment.

Potentiodynamic polarization measurements were carried out on a Solartron electrochemical workstation in a conventional three-electrode cell configuration: a saturated calomel electrode as the reference electrode, a platinum mesh as a counter electrode, and the coated sample as the

working electrode. After the electrochemical testing system became stable, the measurements were carried out in a 3.5 wt% NaCl solution at 25 °C. The scanning rate was 1 mV s<sup>-1</sup>, with a scanning potential range from -0.6 V to +0.6 V versus the open circuit potential.

## Results and discussion

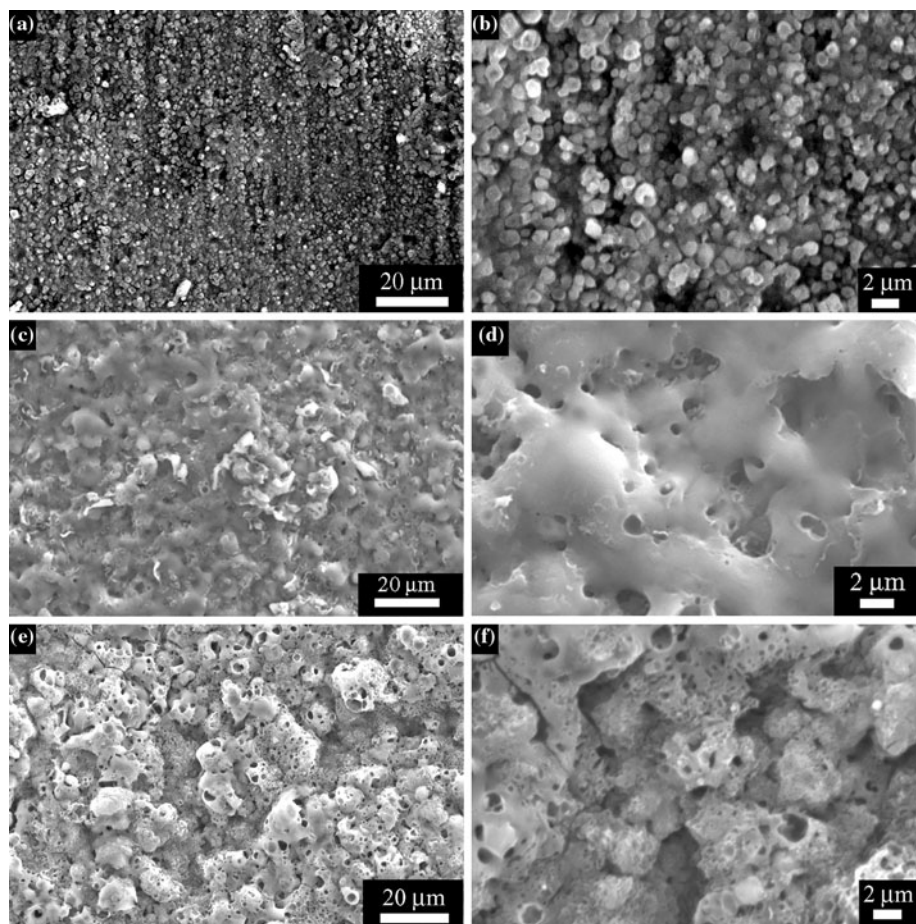
### Effect of duty ratio on the coating microstructure

Usually, duty ratio is an important parameter in controlling the morphology of the coatings because the sparking discharge duration depends on the pulse on-time [29]. Figure 2 shows the surface of the coating at a constant current subjected to different duty ratios, ranging from 10 to 40%. At the lowest duty ratio of 10%, the grains in the coating show spherical particles with smaller sizes, about 1 μm (Fig. 2a, b). Pores are observed in most of the particles (Fig. 2b). At a duty ratio of 20%, the size of grains in the coating is increased and there are also many small pores on the surface, which correspond to the discharge channels on the sample surface during the oxidation process, as shown

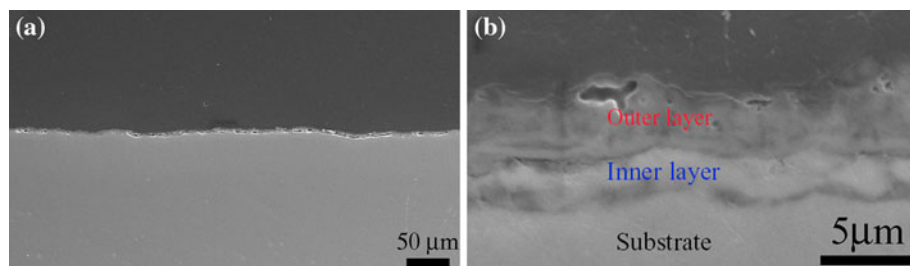
in Fig. 2c. Klapkiv [30] suggested that the instantaneous temperature in these discharge channels can be over several thousands degrees Celsius, where the plasma atmosphere is generated. Under such a high temperature, the oxide coatings on the titanium may be locally and temporarily molten. When the spark or micro-arc quenches, the molten materials in the plasma discharge zone rapidly solidify due to the aqueous solution cooling (Fig. 2d). When the duty ratio is further increased, the discharge time in a single pulse is lengthened, and the current density is accordingly increased, which promotes the grain growth, and results in a coarser coating (Fig. 2e, f). It is observed that many larger grains, accompanied by larger pores and cracks, appear on the surface beyond a duty ratio of 40%.

Figure 3 shows the cross-sectional SEM images of the coating prepared at 900 Hz,  $D = 20\%$ , and  $R = 3$ . As shown in Fig. 3a, it indicates that the coating is continuous and uniform. From the high-magnification SEM image (Fig. 3b), it can be seen that the coating is composed of a two-layer structure, a porous outer layer and a dense inner layer. The pores are found to be present merely in the outer loose layer, but do not traverse through the inner dense layer to the titanium substrate. The two-layer structure can

**Fig. 2** Surface SEM images of the coatings prepared at 900 Hz,  $R = 3$ , and under different duty ratios: **a, b**  $D = 10\%$ ; **c, d**  $D = 20\%$ ; and **e, f**  $D = 40\%$



**Fig. 3** Cross-sectional SEM images of the coatings prepared at 900 Hz,  $D = 20\%$ ,  $R = 3$



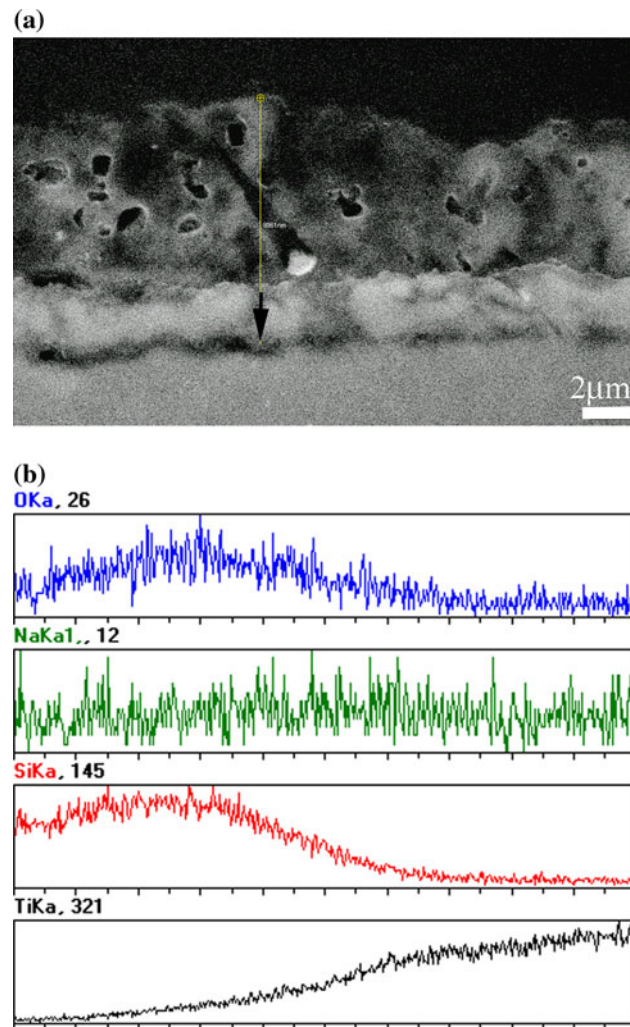
be explained by the existence of different transient temperature fields in the outer and inner layers [31–33]. The fluctuations of surface temperature due to periodical plasma discharges cause repeated melting and solidification in the outer layer, leading to a porous structure. Due to the difficulty of thermal mass of the substrate, the transient temperature in the inner layer is lower than that in the outer layer. The sparking tends to occur on the thinner place where the film is easily broken down. If there are cracks or pores within the dense layer, the sparking will occur at these places, and the cracks and pores would be healed up by the fused oxide, thus there are no cracks or pores in the dense layer.

Figure 4b shows the EDS line profiles of elements scanned along the line marked in Fig. 4a. The gradient distribution of Ti, Si, and O indicates that the relative content of Si decreases, while Ti increases from the coating surface to the titanium substrate. For the inner layer, it is mainly consisted of titanium.

The elemental distribution on the surface of coating is also shown in Fig. 5. It is noted that the local nodules-shaped particles on the surface are composed of more constituents of the electrolyte, such as Si and Na in this study, which is consistent with the above results of scanning profiles of elements across the coating. The presence of elements derived from the electrolyte suggests that it is possible to change the compositions of coating by adjusting the components and concentration of the electrolyte solution.

#### Effect of frequencies on the coating microstructure

Frequency is another key factor in controlling the surface morphology of the coating. Figure 6 shows SEM images of the surface morphologies of the  $\text{TiO}_2$  coatings obtained with  $D = 20\%$ ,  $R = 3$ , and at various frequencies from 900 to 4500 Hz. It shows that the coatings are uniform in the frequency range from 900 to 2700 Hz (Fig. 6a–c). When the frequency is increased to 3600 Hz, the grains grow (Fig. 6d). Upon further increase in the frequency to 4500 Hz, there are many cracks on the surface (Fig. 6e). This indicates that frequency has a prominent effect on the microstructure of coatings prepared by PEO processes. The different surface roughness of coatings obtained at various frequencies is



**Fig. 4** **a** SEM image and **b** line scanning profiles of elements across the coating layer prepared at 900 Hz,  $D = 20\%$ ,  $R = 3$

attributed to the different energy density, which influences the melting and the resultant formation of  $\text{TiO}_2$  coating. At higher frequency, the more frequent melting and solidification may cause the cracks in the coatings.

The thickness of the above five coatings prepared at various frequencies from 900 to 4500 Hz is 14, 15, 15, 17, and 20  $\mu\text{m}$ , respectively. The phases of these coating materials were characterized by XRD. Figure 7 shows the XRD patterns of the five coatings prepared at different

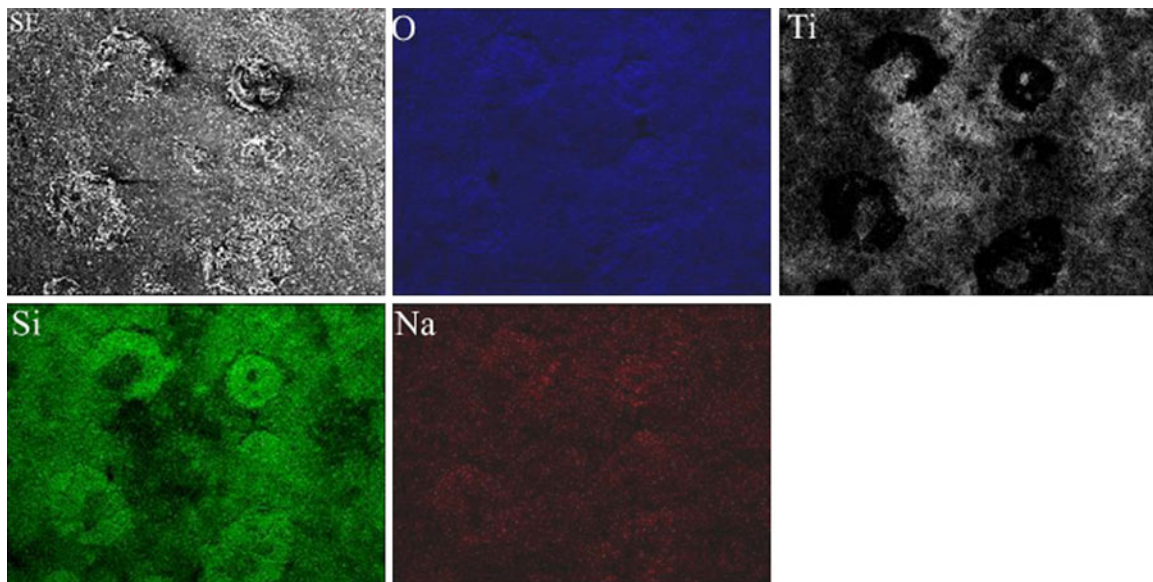
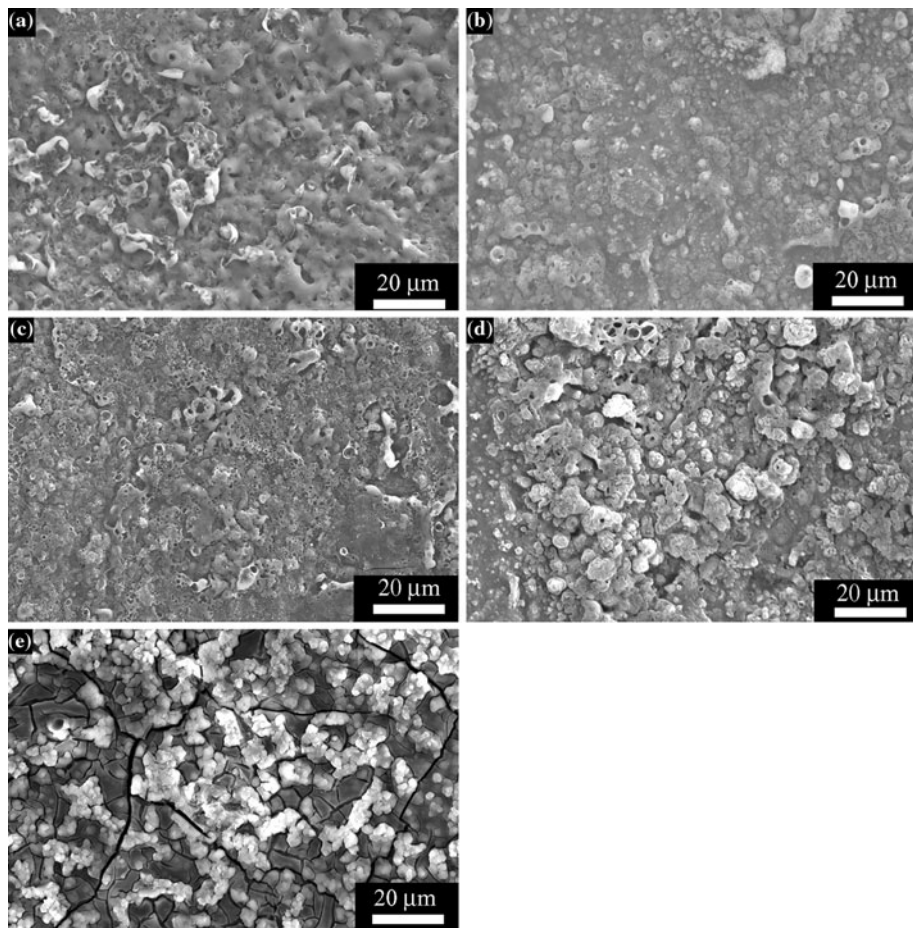


**Fig. 5** Bright-field images and O, Ti, Si, and Na EDX mapping images for surface of ceramic coating prepared at 900 Hz,  $D = 20\%$ ,  $R = 3$

**Fig. 6** Surface SEM images of the coatings prepared under  $D = 20\%$ ,  $R = 3$ , and at different frequencies: **a** 900 Hz; **b** 1800 Hz; **c** 2700 Hz; **d** 3600 Hz; and **e** 4500 Hz



frequencies from 900 to 4500 Hz and the bare titanium substrate. The peaks of titanium in curves b–f come from the titanium substrate, which indicate that the coating is

thin. Besides the peaks from titanium substrate, it shows that the five coatings have similar phases, with the main phases of anatase  $\text{TiO}_2$  (marked with  $\Delta$  in Fig. 7, JCPDS

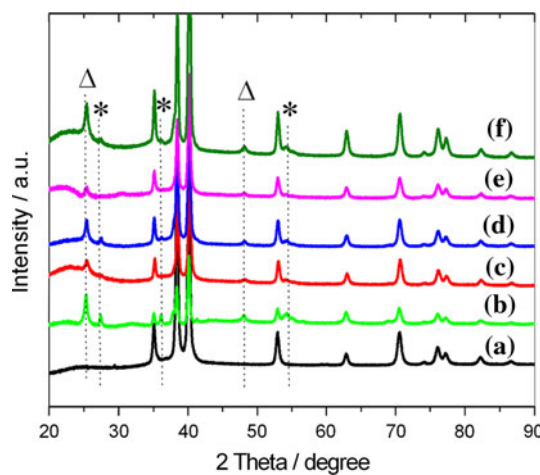
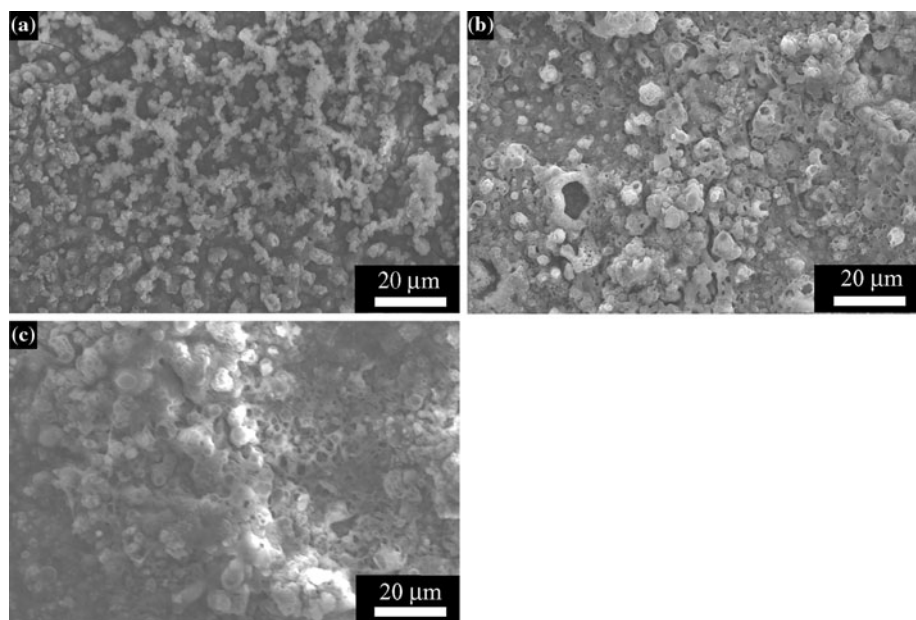


**Fig. 7** XRD patterns of the samples prepared under  $D = 20\%$ ,  $R = 3$ , and at different frequencies: **a** bare titanium substrate; **b** 900 Hz; **c** 1800 Hz; **d** 2700 Hz; **e** 3600 Hz; and **f** 4500 Hz

No. 01-073-1764) plus a little amount of rutile  $\text{TiO}_2$  (marked with \*, JCPDS No. 01-073-1765). Peaks of  $\text{SiO}_2$  were not observed in the XRD patterns. It may be ascribed to the amorphous property and relatively smaller amount of  $\text{SiO}_2$  in the coatings. Colmenares-Angulo et al. [34] have found that the process conditions have great effects on the microstructure, phase content, and physical properties of thermal-sprayed  $\text{TiO}_2$  coatings. Raman spectroscopy may be a very useful tool to characterize various crystalline phase of titania thin films, as observed by Lu et al. [35]. Further study is necessary to understand the process–microstructure–property relationship by means of Raman, TEM, and other characterization methods, which are not in the scope of this article.

**Fig. 8** Surface SEM images of the coatings prepared at 900 Hz,  $D = 20\%$ , and under different  $R$ : **a** 1; **b** 5; and **c** 10



#### Effect of positive/negative pulse proportion on the coating microstructure

The effect of positive/negative pulse proportion ( $R$ ) on the morphology of coatings is also investigated. Figure 8 shows the surface morphology of the coatings prepared using different  $R$  values of 1, 5, and 10. At  $R = 1$ , the coating surface shows island-shape microstructure (Fig. 8a). From the cross-sectional images (data not shown), it also indicates that the coating is not continuous. It is generally believed that the positive portion of alternating pulses promotes the coating growth, whereas the negative portion prevents the growth of a passive oxide [36]. This may be the reason for the discontinuous microstructure observed in the coating prepared at  $R = 1$ .

It is well known that the sparking discharge intensity depends on the pulse energy. Therefore, a change in the pulse ratio can adjust the surface discharge characteristics, which influences the grain growth and microstructure of the coatings. As  $R$  increases, the discharge intensity is increased. Therefore, the accumulated mass of oxide produced by single pulse increases, which induces grain growth. Figure 8b, c shows that the coating surface becomes coarser as  $R$  increases. However, the effect of  $R$  on the microstructure of coatings is not so obvious compared to those of duty ratio and frequency.

#### Corrosion-resistant properties of the ceramic coating

The coating sample with uniform and crack-free microstructure prepared at 900 Hz,  $D = 20\%$ ,  $R = 3$ , was selected for corrosion resistance test. The potentiodynamic

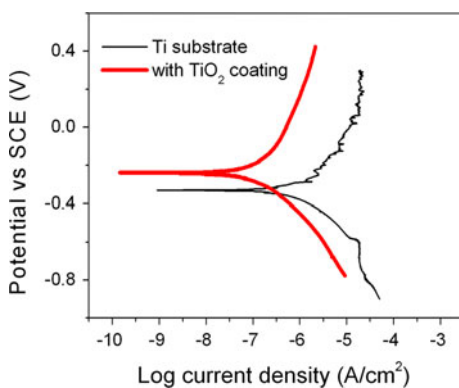


**Fig. 9** Potentiodynamic polarization curves of the titanium substrate and coated sample prepared at 900 Hz,  $D = 20\%$ , and  $R = 3$ ; tested in 3.5% NaCl solution

polarization curves of the coated sample and the bare titanium substrate are shown in Fig. 9. It can be seen that the corrosion potential ( $E_{\text{corr}}$ ) rises from  $-0.378$  V for bare titanium substrate to  $-0.251$  V for the coated sample; whereas the corrosion current density ( $i_{\text{corr}}$ ) decreases about one-order magnitude. The results clearly demonstrate that the coated sample has better corrosion-resistant property than the bare substrate due to the existence of the ceramic coatings.

## Conclusions

In summary,  $\text{TiO}_2$  coatings have successfully been prepared on titanium substrates by PEO. The coatings are mainly consisted of anatase  $\text{TiO}_2$  phase and a little amount of rutile phase. It was found that process parameters have great effects on the surface morphologies of coatings, intrinsically by altering the energy input. The coatings obtained at the frequency range 900–2700 Hz, under a duty ratio of 20%, and a positive/negative pulse proportion of 3, are crack-free, dense, and well bonded. The effect of positive/negative pulse proportion is relatively small; however, continuous coatings have not been obtained using the  $R$  value of 1. The corrosion-resistance property of titanium was obviously improved by  $\text{TiO}_2$  coatings formed by the PEO process.

Further work on understanding the effect of electrolyte solution composition on the microstructure of the ceramic coatings and oxidation mechanism is in progress. The results obtained in this study provide some insights into the optimization of the PEO processes to obtain ceramic coatings on other light metals or alloy substrates.

**Acknowledgements** The authors acknowledge the financial support from the Canadian National Program on Generation IV Energy Technologies. The authors would like to thank Tom Vanderhoek for the preparation of metallic substrates.

## References

- Brewer WD, Bird RK, Wallace TA (1998) Mater Sci Eng A 243:299
- Tjong SC, Mai YW (2008) Compos Sci Technol 68:583
- Yamashita Y, Takayama I, Fujii H, Yamazai T (2002) Nippon Steel Tech Rep 85:11
- Cannillo V, Colmenares-Angulo J, Lusvarghi L, Pierli F, Sampath S (2009) J Eur Ceram Soc 29:1665
- Matykina E, Arrabal R, Skeldon P, Thompson GE (2009) Acta Biomater 5:1356
- Geetha M, Singh AK, Asokamani R, Gogia AK (2009) Prog Mater Sci 54:397
- Schutz RW, Watkins HB (1998) Mater Sci Eng A 243:305
- Rahman M, Wang ZG, Wong YS (2006) JSME Int J Ser C 49:11
- Wang YM, Jia DC, Guo LX, Lei TQ, Jiang BL (2005) Mater Chem Phys 90:128
- Moskalewicz T, Smeacetto F, Czyska-Filemonowicz A (2009) Surf Coat Technol 203:2249
- Kalita VI, Gnedovets AG (2005) Plasma Process Polym 2:485
- Cammarota GP, Casagrande A, Poli G, Veronesi P (2009) Surf Coat Technol 203:1429
- Yang W, Hsu M, Lin M, Chen Z, Chen L, Huang H (2009) J Alloys Compd 479:642
- Teng S, Liang W, Li Z, Ma X (2008) J Alloys Compd 464:452
- Zhang XJ, Gao YH, Ren BY, Tsubaki N (2010) J Mater Sci 45:1622. doi:[10.1007/s10853-009-4138-8](https://doi.org/10.1007/s10853-009-4138-8)
- Fritzsche A, Haenle M, Zietz C, Mittelmeier W, Neumann H, Heidenau F, Finke B, Bader R (2009) J Mater Sci 44:5544. doi:[10.1007/s10853-009-3776-1](https://doi.org/10.1007/s10853-009-3776-1)
- Gong S, Xu H, Yu Q, Zhou C (2000) Surf Coat Technol 130:128
- Yerokhin AL, Nie X, Leyland A, Matthews A, Dowey SJ (1999) Surf Coat Technol 122:73
- Parfenov EV, Yerokhin AL, Matthews A (2007) Thin Solid Films 516:428
- Zhao Z, Chen X, Chen A, Huo G, Li H (2009) J Mater Sci 44:6310. doi:[10.1007/s10853-009-3869-x](https://doi.org/10.1007/s10853-009-3869-x)
- Xue W, Deng Z, Chen R, Zhang T (2000) Thin Solid Films 372:114
- Yerokhin AL, Nie X, Leyland A, Matthews A (2000) Surf Coat Technol 130:195
- Xue W, Wang C, Deng Z, Zhang T (2002) ISIJ Int 42:651
- Han Y, Hong SH, Xu KW (2002) Surf Coat Technol 154:314
- Matykina E, Skeldon P, Thompson GE (2007) Surf Eng 23:412
- Birss V, Xia S, Yue R, Rateck RG Jr (2004) J Electrochem Soc 151:B1
- Han Y, Hong S, Xu K (2003) Surf Coat Technol 168:249
- Yao Z, Cui R, Jiang Z, Wang F (2007) Appl Surf Sci 253:6778
- Rudnev VS, Yarovaya TP, Lysenko AE, Nedosorov PM, Dushina NE (2008) Prot Met 44:715
- Klapkiv MD (1995) Mater Sci 31:494
- Gu WC, Lv GH, Chen H, Chen GL, Feng WR, Yang SZ (2007) Mater Sci Eng A 447:158
- Teh TH, Berkani A, Mato S, Skeldon P, Thompson GE, Habazaki H, Shimizu K (2003) Corros Sci 45:2757
- Guan Y, Xia Y, Li G (2008) Surf Coat Technol 202:4602
- Colmenares-Angulo JR, Cannillo V, Lusvarghi L, Sola A, Sampath S (2009) J Mater Sci 44:2276. doi:[10.1007/s10853-008-3044-9](https://doi.org/10.1007/s10853-008-3044-9)
- Lu SW, Harris C, Walck S, Arbab M (2009) J Mater Sci 44:541. doi:[10.1007/s10853-008-3086-z](https://doi.org/10.1007/s10853-008-3086-z)
- Erokhine A, Voevodin AA, Schmertzler RD (1998) US Patent 5,720,866